PROCEEDINGS OF SCIENCE

Correlated Dirac Eigenvalues and Axial Anomaly in Chiral Symmetric QCD

H.-T. Ding,[1] S.-T. Li,[1] Swagato Mukherjee,[2] A. Tomiya,[3] X.-D. Wang[1] and Y. Zhang[4,*]

[1] *Key Laboratory of Quark & Lepton Physics (MOE) and Institute of Particle Physics, Central China Normal University, Wuhan 430079, China*

[2] *Physics Department, Brookhaven National Laboratory, Upton, NY 11973, USA*

[3] *RIKEN-BNL Research Center, Brookhaven National Laboratory, Upton, New York 11973, USA*

[4] *RIKEN Center for Computational Science, 7-1-26 Minatojima-minami-machi, Chuo-ku, Kobe, Hyogo 650-0047, Japan*

E-mail: hengtong.ding@mail.ccnu.edu.cn, lishengtai@mails.ccnu.edu.cn, akio.tomiya@riken.jp, swagato@bnl.gov, xiaodanwang@mails.ccnu.edu.cn, yu.zhang.ey@riken.jp

We investigate the Dirac eigenvalue spectrum ($\rho(\lambda, m_l)$) to study the microscopic origin of axial anomaly in high temperature phase of QCD. We propose novel relations between the derivatives ($\partial^n \rho(\lambda, m_l)/\partial m_l^n$) of the Dirac eigenvalue spectrum with respect to the quark mass (m_l) and the (n+1)-point correlations among the eigenvalues (λ) of the massless Dirac operator. Based on these relations, we present lattice QCD results for $\partial^n \rho(\lambda, m_l)/\partial m_l^n$ ($n = 1, 2, 3$) with m_l corresponding to pion masses $m_\pi = 160 - 55$ MeV, and at a temperature of about 1.6 times the chiral phase transition temperature. Calculations were carried out using (2+1)-flavors of highly improved staggered quarks and the tree-level Symanzik gauge action with the physical strange quark mass, three lattice spacings $a = 0.12, 0.08, 0.06$ fm, and lattices having aspect ratios $4 - 9$. We find that $\rho(\lambda \to 0, m_l)$ develops a peaked structure. This peaked structure, which arises due to non-Poisson correlations within the infrared part of the Dirac eigenvalue spectrum, becomes sharper as $a \to 0$, and its amplitude is proportional to m_l^2. After continuum and chiral extrapolations, we find that the axial anomaly remains manifested in two-point correlation functions of scalar and pseudo-scalar mesons in the chiral limit. We demonstrate that the behavior of $\rho(\lambda \to 0, m_l)$ is responsible for it.

The 38th International Symposium on Lattice Field Theory, LATTICE2021 26th-30th July, 2021 Zoom/Gather@Massachusetts Institute of Technology

[*] Speaker

© Copyright owned by the author(s) under the terms of the Creative Commons Attribution-NonCommercial-NoDerivatives 4.0 International License (CC BY-NC-ND 4.0).

PoS(LATTICE2021)619

1. Introduction

The Lagrangian of the (2+1)-flavor Quantum Chromodynamics (QCD) has a global symmetry $SU(2)_{\mathrm{L}} \times SU(2)_{\mathrm{R}} \times U(1)_{\mathrm{A}} \times U(1)_V$ in the classic limit and the chiral limit of $m_l \to 0$. The $SU(2)_{\mathrm{L}} \times SU(2)_{\mathrm{R}}$ chiral symmetry is spontaneously broken in the vacuum and the $U(1)_{\mathrm{A}}$ symmetry is anomalously broken on the quantum level due to the Adler-Bell-Jackiw or chiral anomaly. For the physical m_l lattice simulations have established quite firmly that QCD transition is a rapid cross over at a pesudocritical temperature at $T \simeq 156$ MeV [1–3], while in the chiral limit $m_l \to 0$ chiral phase transition temperature at which the $SU(2)_{\mathrm{L}} \times SU(2)_{\mathrm{R}}$ is restored is estimated as $T_c = 132^{+3}_{-6}$ MeV based on the O(4) scaling analyses [4].

Conversely, the fate of the $U(1)_{\mathrm{A}}$ symmetry in the high temperature phase of QCD remains unclear. Although the quantum anomaly is present at any finite temperature, at some point its effects could become negligible due to the asymptotic restoration of the $U(1)_{\mathrm{A}}$ symmetry with the temperature, thus the $U(1)_{\mathrm{A}}$ symmetry would be effectively restored. The order of the chiral transition and the associated universality class is known to depend crucially on how axial anomaly manifests itself in the two-point correlation functions of light scalar and pseudoscalar mesons for $T \geq T_c$. If the isotriplet scalar δ and the isotriplet pseudoscalar π remain non-degenerate at $T \geq T_c$, then we expect a second order phase transition which belongs to the three-dimensional $O(4)$ universality class [5]. But if the δ and π become degenerate at $T \geq T_c$, then the chiral phase transition can be either first [5] or second order with the symmetry breaking pattern $U(2)_V \times U(2)_A \to U(2)_V$ universality class [6, 7]. For the physical m_l, the δ and π remain nondegenerate around the chiral crossover [2, 8, 9]. However, what happens for $T \simeq T_c$ as $m_l \to 0$ remains an open question [10–13] due to the lack of state-of-the-art lattice QCD calculations with controlled continuum and chiral extrapolations.

To gain more insight about the microscopic origin of the axial anomaly we can investigate the Dirac eigenvalue spectrum $\rho(\lambda, m_l)$. It has been shown that if $\rho(\lambda, m_l)$ is an analytic function of m_l^2 and λ then in the chiral limit $U(1)_{\mathrm{A}}$ breaking effects are invisible in differences of up to 6-point correlation functions of π and δ that can be connected via a $U(1)_{\mathrm{A}}$ rotation [14]. However, the dilute instanton gas approximation (DIGA) [15] predicated that $\rho \sim m_l^2 \delta(\lambda)$ can lead to nondegeneracy of the two-point π and δ correlation functions even as $m_l \to 0$ [16–18]. Some lattice QCD studies have observed infrared enhancement in ρ [8, 11, 16], however, whether such enhancements scale as m_l^2 as $m_l \to 0$ have not been demonstrated. In other lattice QCD calculations, no infrared enhancement in ρ was observed [12, 19, 20], showing the importance of controlling lattice artifacts through continuum extrapolations. On the other hand, in Ref. [21] it was argued that if π and δ were to remain nondegenerate at $T \geq T_c$, then chiral symmetry restoration demands non-Poisson correlations among the infrared eigenvalues.

In this work we propose the novel relation between $\partial^n \rho / \partial m_l^n$ and correlation among the eigenvalues to investigate the microscopic origin of axial anomaly at high temperature phase. The rest of paper is organized as follows. We describe the basic idea of how to obtain the relation between $\partial^n \rho / \partial m_l^n$ and correlation among the eigenvalues in section 2. In section 3 we show the setup of our lattice simulations. We then show our numerical results in Section 4. Finally we present our conclusion in Section 5. The detailed information about this work can be found in [22].

PoS(LATTICE2021)619

2. $\partial^n\rho/\partial m_l^n$ & C_{n+1} and $U(1)_A$ anomaly

For (2+1)-flavor QCD, the Dirac eigenvalue spectrum is given by

$$\rho(\lambda, m_l) = \frac{T}{VZ[\mathcal{U}]}\int \mathcal{D}[\mathcal{U}]e^{-S_G[\mathcal{U}]}\det\left[\not{D}[\mathcal{U}]+m_s\right]\left(\det\left[\not{D}[\mathcal{U}]+m_l\right]\right)^2\rho_U(\lambda)\,. \tag{1}$$

Here $\rho_U(\lambda)$ is the Dirac eigenvalue spectrum for a given gauge configuration, It is defined as $\rho_U(\lambda)=\sum_j\delta(\lambda-\lambda_j)$, λ_j are the eigenvalues of the massless Dirac matrix $\not{D}[\mathcal{U}]$. Note that $\rho_U(\lambda)$ does not explicitly depend on m_l and the m_l dependence is embedded in the determinant term. Furthermore,

$$\det\left[\not{D}[\mathcal{U}]+m_l\right] = \prod_j\left(+\mathrm{i}\,\lambda_j+m_l\right)\left(-\mathrm{i}\,\lambda_j+m_l\right) = \exp\left(\int_0^\infty \mathrm{d}\lambda\,\rho_U(\lambda)\ln\left[\lambda^2+m_l^2\right]\right). \tag{2}$$

Substituting Eq. 2 in Eq. 1 and $Z[\mathcal{U}]$ it is straightforward to obtain $\partial^n\rho/\partial m_l^n$ [22], e.g.,

$$\frac{V}{T}\frac{\partial\rho}{\partial m_l} = \int_0^\infty \mathrm{d}\lambda_2\frac{4m_l\,C_2(\lambda,\lambda_2;m_l)}{\lambda_2^2+m_l^2}\,, \tag{3}$$

$$\frac{V}{T}\frac{\partial^2\rho}{\partial m_l^2} = \int_0^\infty \mathrm{d}\lambda_2\,\frac{4(\lambda_2^2-m_l^2)\,C_2(\lambda,\lambda_2;m_l)}{\left(\lambda_2^2+m_l^2\right)^2} + \int_0^\infty d\lambda_3\int_0^\infty d\lambda_2\frac{(4m_l)^2\,C_3(\lambda,\lambda_2,\lambda_3;m_l)}{\left(\lambda_2^2+m_l^2\right)\left(\lambda_3^2+m_l^2\right)}\,, \tag{4}$$

$$\text{with}\quad C_n(\lambda_1,\cdots,\lambda_n;m_l) = \left\langle\prod_{i=1}^n\left[\rho_U(\lambda_i)-\langle\rho_U(\lambda_i)\rangle\right]\right\rangle. \tag{5}$$

The difference of the integrated two-point functions in the pion and delta channel is defined as

$$\chi_\pi-\chi_\delta = \int \mathrm{d}^4x\left\langle\pi^i(x)\pi^i(0)-\delta^i(x)\delta^i(0)\right\rangle\,. \tag{6}$$

For $T\geq T_c$ owing to the degeneracy of π and the σ in the chiral limit [16]

$$\chi_\pi-\chi_\delta = \chi_{\mathrm{disc}}\,, \tag{7}$$

where χ_{disc} is the quark-line disconnected part of the isosinglet scalar meson susceptibility,

$$\chi_{\mathrm{disc}} = \frac{T}{V}\int \mathrm{d}^4x\left\langle\left[\bar\psi(x)\psi(x)-\langle\bar\psi(x)\psi(x)\rangle\right]^2\right\rangle\,. \tag{8}$$

The $\mathrm{U}(1)_\mathrm{A}$ symmetry-breaking measures $\chi_\pi-\chi_\delta$ and χ_{disc} are related to ρ through [16, 22]

$$\chi_\pi-\chi_\delta = \int_0^\infty \mathrm{d}\lambda\,\frac{8m_l^2\,\rho}{\left(\lambda^2+m_l^2\right)^2}\,,\qquad \chi_{\mathrm{disc}} = \int_0^\infty \mathrm{d}\lambda\,\frac{4m_l\;\partial\rho/\partial m_l}{\lambda^2+m_l^2}\,. \tag{9}$$

In the Poisson limit, $C_n^{\mathrm{Po}}(\lambda_1,\cdots,\lambda_n)=\delta(\lambda_1-\lambda_2)\cdots\delta(\lambda_n-\lambda_{n-1})\left\langle(\rho_U(\lambda_1)-\langle\rho_U(\lambda_1)\rangle)^n\right\rangle = \delta(\lambda_1-\lambda_2)\cdots\delta(\lambda_n-\lambda_{n-1})\left\langle\rho_U(\lambda_1)\right\rangle+O(1/N)$, where $2N\propto V/T$ is the total number of eigenvalues. In this limit the first and second order quark mass derivatives of ρ are expressed as follows

$$\left(\frac{\partial\rho}{\partial m_l}\right)^{\mathrm{Po}} = \frac{4m_l\rho}{\lambda^2+m_l^2}-\frac{V\rho}{TN}\left\langle\bar\psi\psi\right\rangle\,, \tag{10}$$

$$\left(\frac{\partial^2\rho}{\partial m_l^2}\right)^{\mathrm{Po}} = \frac{4\rho}{\lambda^2+m_l^2}+\frac{8m_l^2\rho}{\left(\lambda^2+m_l^2\right)^2}+\frac{2V^2\rho}{T^2N^2}\left\langle\bar\psi\psi\right\rangle^2-\frac{V\rho}{TN}\left(\frac{8m_l\left\langle\bar\psi\psi\right\rangle}{\lambda^2+m_l^2}+2\chi_\pi-\chi_\delta\right), \tag{11}$$

PoS(LATTICE2021)619

In the chiral limit, this leads to $\chi_{\rm disc}^{\rm Po} = 2(\chi_\pi - \chi_\delta)$, in clear violation of the chiral symmetry restoration condition in Eq. 7, unless both sides of the equation trivially vanish.

3. Lattice setup

Lattice QCD calculations were carried out at $T \approx 205$ MeV $\approx 1.6T_c$ for (2+1)-flavor QCD using the highly improved staggered quarks and the tree-level Symanzik gauge action. The m_s was tuned to its physical value, and three lattice spacings $a = (TN_\tau)^{-1} = 0.12, 0.08, 0.06$ fm corresponding to $N_\tau = 8, 12, 16$, were used [22]. Calculations were done with $m_l = m_s/20, m_s/27, m_s/40, m_s/80,$ $m_s/160$ that correspond to $m_\pi \simeq 160, 140, 110, 80, 55$ MeV, respectively. The spatial extents (N_σ) of the lattices were chosen to have aspect ratios in the range of $N_\sigma/N_\tau = 4 - 9$. ρ and C_n were computed by measuring $\rho_U(\lambda)$ over the entire range of λ using the Chebyshev filtering technique combined with the stochastic estimate method [23–26] on about 2000 configurations where each configuration is separated by 10 time units. Orders of the Chebyshev polynomials were chosen to be $(1-5)\times 10^5$ and 24 Gaussian stochastic sources were used. Measurements of $\chi_{\rm disc}$ and $\chi_\pi - \chi_\delta$ were done by inverting the light fermion matrix using 50 Gaussian random sources on $2000-10000$ configurations. Apart from the data sets as shown in above which were reported in [22], in this paper we also add new results based on simulations with $m_l = m_s/160$ on $N_\tau = 12, 16$ lattices. For each of these two parameter sets 4200-5200 configurations each separated by 10 time units are generated, and $\chi_{\rm disc}$ and $\chi_\pi - \chi_\delta$ are measured by inverting the fermion matrix on these configurations.

4. Results

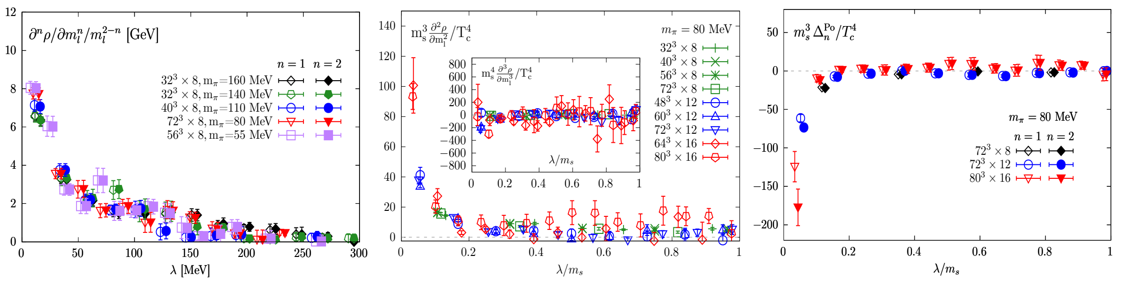

Figure 1: Left: m_l dependence of $m_l^{-1}\,\partial\rho(\lambda,m_l)/\partial m_l$ and $\partial^2\rho(\lambda,m_l)/\partial m_l^2$ using $N_\tau = 8$ lattices. Middle: a and V dependence of $\partial^2\rho(\lambda,m_l)/\partial m_l^2$ and $\partial^3\rho(\lambda,m_l)/\partial m_l^3$ (inset) for $m_\pi = 80$ MeV. Right: The differences $\Delta_n^{\rm Po} = m_l^{n-2}\left[\partial^n\rho/\partial m_l^n - (\partial^n\rho/\partial m_l^n)^{\rm Po}\right]$ for $m_\pi = 80$ MeV and three lattice spacings.

Fig. 1 (left) shows the m_l dependence of $m_l^{-1}\partial\rho/\partial m_l$ and $\partial^2\rho/\partial m_l^2$ at $T \approx 1.6T_c$, obtained on $N_\tau = 8$ and the largest available N_σ for that m_l. We observe that $m_l^{-1}(\partial\rho/\partial m_l)$ and $\partial^2\rho/\partial m_l^2$ are almost equal to each other and independent of m_l. Also, $m_l^{-1}\partial\rho/\partial m_l$ and $\partial^2\rho/\partial m_l^2$ develops a peak at $\lambda \to 0$ and it drops rapidly toward zero for $\lambda/T \gtrsim 1$. Fig. 1 (middle) depicts the lattice spacing and volume dependence of $\partial^2\rho/\partial m_l^2$ and $\partial^3\rho/\partial m_l^3$ for $m_\pi = 80$ MeV. To compare these quantities across different lattice spacings we multiply with the appropriate powers of m_s to make them renormalization group invariant and make them dimensionless by rescaling with appropriate powers of $T_c = 132$ MeV. We see that the peaked structure in $\partial^2\rho/\partial m_l^2$ at $\lambda \to 0$

PoS(LATTICE2021)619

becomes sharper as $a \longrightarrow 0$, and shows little volume dependence. Moreover, $\partial^3\rho/\partial m_l^3$ are found to be consistent with zero within errors. The findings $m_l^{-1}\partial\rho/\partial m_l \approx \partial^2\rho/\partial m_l^2$ and $\partial^3\rho/\partial m_l^3 \approx 0$ show that the peaked structure $\rho(\lambda \longrightarrow 0, m_l \longrightarrow 0) \propto m_l^2$. In Fig. 1 (right) we show the difference $\Delta_n^{\mathrm{Po}} = m_l^{n-2}\left[\partial^n\rho/\partial m_l^n - (\partial^n\rho/\partial m_l^n)^{\mathrm{Po}}\right]$ $(n = 1, 2)$, with the Poisson approximations for $\partial^n\rho/\partial m_l^n$ as defined in Eq. 10 and Eq. 11. The fact $\Delta_n^{\mathrm{Po}} < 0$ shows that the repulsive non-Poisson correlation within the small λ gives rise to the $\rho(\lambda \longrightarrow 0)$ peak.

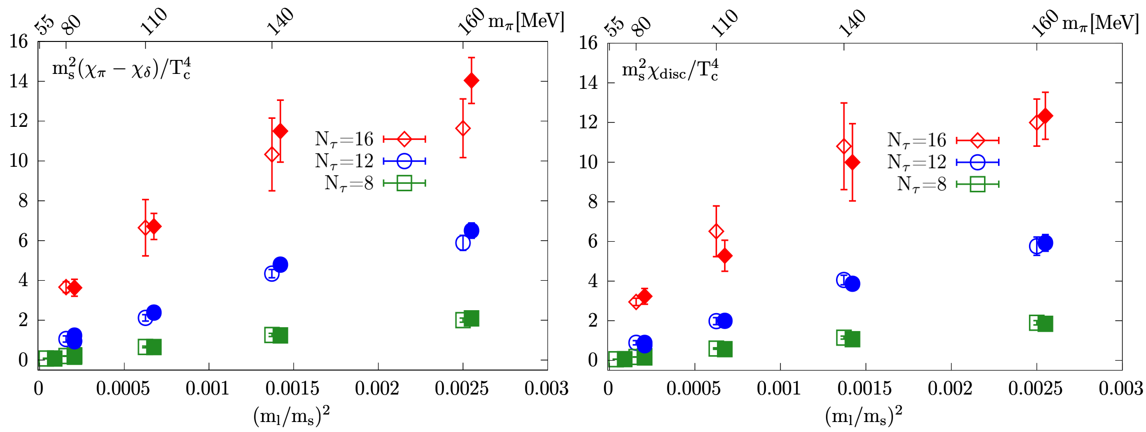

Figure 2: Comparisons of direct measurements (open symbols) of $\chi_\pi - \chi_\delta$ (left) and χ_{disc} (right) with those reconstructed (filled symbols, slightly shifted horizontally for visibility) from ρ and $\partial\rho/\partial m_l$ using Eq. 9.

In Fig. 2 we show that ρ and $\partial\rho/\partial m_l$ reproduce directly measured $\chi_\pi - \chi_\delta$ and χ_{disc} using Eq. 9. We checked that only the infrared $\lambda/T \lesssim 1$ parts of ρ and $\partial\rho/\partial m_l$ are needed for the reproductions of $\chi_\pi - \chi_\delta$ and χ_{disc}. Additionally, we checked that once the bin-size of λ in the numerical integration of left equation of Eq. 9 is chosen to reproduce directly measured $\chi_\pi - \chi_\delta$, the same bin size automatically reproduces χ_{disc} and $\langle\bar\psi\psi\rangle$ without any further tuning.

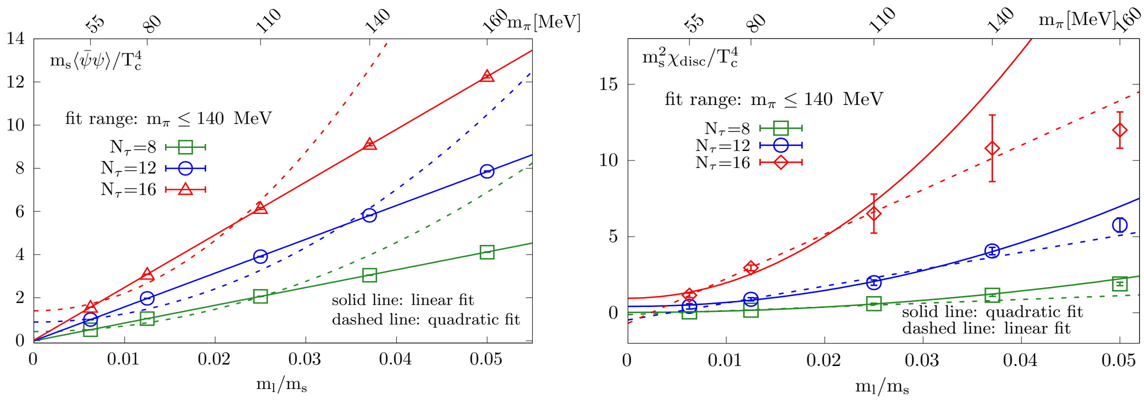

Figure 3: Left: $m_s\langle\bar\psi\psi\rangle/T_c^4$ as a function of quark mass for three lattice spacings with two different fit ansatz. The solid lines denote linear fits in quark mass while the dashed lines denote quadratic fits in quark mass. Right: Same as the left one but for $m_s^2\chi_{\mathrm{disc}}/T_c^4$. Here the solid lines denote quadratic fits while the dashed lines represent linear fits in quark mass.

In the left panel of Fig. 3 we show the quark mass dependence of chiral condensate in detail. We performed linear fits (solid lines) and a quadratic fits (dotted lines) in quark mass to the chiral

PoS(LATTICE2021)619

condensate. It can be clearly seen that the linear fits give a good description of the data and the fit result of chiral condensates at each lattice spacing vanish in the chiral limit. This is in accord with the expectation $Z[\mathcal{U}]$ is an even function of m_l for $T \geq T_c$ due to the restoration of the $Z(2)$ subgroup of $SU(2)_\mathrm{L} \times SU(2)_\mathrm{R}$ [1]. This leads to the expectation that the χ_disc should be quadratic in quark mass as $m_l \to 0$. As can be seen from the right panel of Fig. 3 which shows the $m_s^2 \chi_\mathrm{disc}/T_c^4$ as a function of quark mass for $N_\tau = 8, 12, 16$, the data indeed favors the quadratic dependence of $m_s^2 \chi_\mathrm{disc}/T_c^4$ in quark mass as $m_l \to 0$.

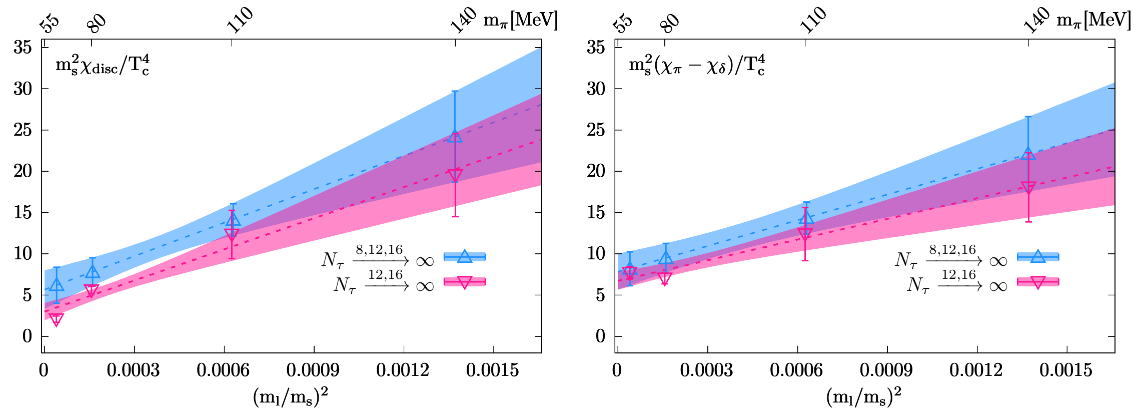

Figure 4: Continuum and chiral extrapolated results for χ_disc (left) and $\chi_\pi - \chi_\delta$ (right) at $T \approx 205$ MeV. See text for details.

In Fig. 4 we show the continuum and chiral extrapolated results for χ_disc and $\chi_\pi - \chi_\delta$. With the additional 2 data points at $m_s/m_l = 160$ (or $m_\pi = 55$ MeV) on N_τ= 12 and 16, we follow the same analysis methods as in our previous studies [22]. I.e. using data for $N_\tau = 8, 12, 16$ and $m_\pi \leq 140$ MeV, we performed a joint $a, m_l \to 0$ extrapolation of the form $\chi_\mathrm{disc}(a, m_l) = \chi_\mathrm{disc}(0,0) + a_1/N_\tau^2 + a_2/N_\tau^4 + (m_l/m_s)^2\left[b_0 + b_1/N_\tau^2 + b_2/N_\tau^4\right]$. Fits were performed on each bootstrap sample of the data set. The bootstrap samples were created by randomly choosing data from Gaussian distributions with means equal to the average values and variances equal to the errors of χ_disc. We chose the median value as the final result (depicted by the upward triangles) and the 68% percentiles confidence interval of the resulting bootstrap distribution as the errors (the band labeled by $N_\tau \xrightarrow{8,12,16} \infty$). Since we used the so-called rooted-staggered formulation [27], we also checked that the same $\chi_\mathrm{disc}(0,0)$ is obtained within errors by first carrying out the $a \to 0$ extrapolations for each m_l and then performing the $m_l \to 0$ extrapolation. For this purpose, we used the $N_\tau = 12, 16$ data for each of $m_l = m_s/27, m_s/40, m_s/80, m_s/160$ to obtain $\chi_\mathrm{disc}(0, m_l)$ by fitting to the ansatz $\chi_\mathrm{disc}(a, m_l) = \chi_\mathrm{disc}(0, m_l) + d_1/N_\tau^2$. Then the chiral extrapolation was carried out using $\chi_\mathrm{disc}(0, m_l) = \chi_\mathrm{disc}(0,0) + d_2(m_l/m_s)^2$ based on the continuum estimates of $\chi_\mathrm{disc}(0, m_l)$. These extrapolations were done by using the same bootstrap procedure described before and the final results are indicated with the label $N_\tau \xrightarrow{12,16} \infty$. The same procedures were followed also for $\chi_\pi - \chi_\delta$ to obtain its continuum and chiral extrapolated values. After carrying out continuum and chiral extrapolations we obtained that $\chi_\mathrm{disc}(0,0)$ is 3.0 ± 1.1 for the sequential fit and 5.7 ± 2.3 for the joint fit, which is 2-3 σ away from 0, while $[\chi_\pi - \chi_\delta](0,0)$ is 6.7 ± 1.1 for the sequential fit

[1]In the staggered discretization formalism the remnant chiral symmetry at nonzero lattice spacing is O(2).

PoS(LATTICE2021)619

and 7.8 ± 2.2 for the joint fit, which is 4-6 σ away from 0. We find that Eq. 7 is satisfied within errors, and $\chi_{\rm disc}$ and $\chi_\pi - \chi_\delta$ are nonvanishing at a confidence level above 95%. These results are consistent with those obtained without the two additional data points [22].

5. Conclusions

In this work we establish relations between $\partial^n\rho/\partial m_l^n$ and C_{n+1}. Based on these relations, we present direct computations of $\partial^n\rho/\partial m_l^n$ employing state-of-the-art lattice QCD techniques. Based on these results we conclude that, in chiral symmetric (2+1)-flavor QCD at $T \approx 1.6T_c$, (i) $\rho(\lambda \to 0, m_l)$ develops a peaked structure due to repulsive non-Poisson correlations within small λ; the peak becomes sharper as $a \to 0$, and its amplitude is $\propto m_l^2$. (ii) The underlying presence of this $\rho(\lambda \to 0, m_l)$ leads to manifestations of $U(1)_{\rm A}$ anomaly in $\chi_\pi - \chi_\delta$ and $\chi_{\rm disc}$. (iii) Axial anomaly remains manifested in $\chi_\pi - \chi_\delta$ and $\chi_{\rm disc}$ even in the chiral limit. These suggest that for $T \sim 1.6T_c$ the microscopic origin of axial anomaly is driven by the weakly interacting (quasi)instanton gas motivated $\rho(\lambda \to 0, m_l \to 0) \sim m_l^2\delta(\lambda)$, and the chiral phase transition in (2+1)-flavor QCD is of the three-dimensional $O(4)$ universality class.

The above conclusions are based on the continuum extrapolated lattice QCD calculations using the (2+1) flavors of staggered fermions. Confirmations of these continuum extrapolated results using other fermion actions, especially using chiral fermions, are needed in future. Even in those future calculations it will be very difficult to directly identify a structure like $m_l^2\delta(\lambda)$ in ρ itself as $m_l \to 0$. The formalism developed and techniques presented in this work for directly accessing $\partial^n\rho/\partial m_l^n$ will be essential for those future studies too.

Acknowledgement

This material is based upon work supported by the National Natural Science Foundation of China under Grants No. 11775096, No. 11535012, and No. 11947237; the U.S. Department of Energy, Office of Science, Office of Nuclear Physics through the Award No. DE-SC0012704; the U.S. Department of Energy, Office of Science, Office of Nuclear Physics and Office of Advanced Scientific Computing Research within the framework of Scientific Discovery through Advance Computing (SciDAC) award Computing the Properties of Matter with Leadership Computing Resources; and RIKEN Special Postdoctoral Researcher program and JSPS KAKENHI Grant No. JP20K14479. Computations for this work were carried out on the GPU clusters of the Nuclear Science Computing Center at Central China Normal University (NSC^3), Wuhan, China, and facilities of the USQCD Collaboration, which are funded by the Office of Science of the U.S. Department of Energy. For generating the gauge configurations, the HotQCD software suite was used, and the eigenvalue measurement code was developed also based on the same software suite. We are indebted to the HotQCD Collaboration for sharing their software suite with us.

References

[1] Y. Aoki, S. Borsanyi, S. Durr, Z. Fodor, S.D. Katz, S. Krieg et al., *The QCD transition temperature: results with physical masses in the continuum limit II.*, *JHEP* **06** (2009) 088 [0903.4155].

PoS(LATTICE2021)619

[2] T. Bhattacharya, M.I. Buchoff, N.H. Christ, H.-T. Ding, R. Gupta et al., *QCD Phase Transition with Chiral Quarks and Physical Quark Masses*, *Phys.Rev.Lett.* **113** (2014) 082001 [1402.5175].

[3] HotQCD collaboration, *Chiral crossover in QCD at zero and non-zero chemical potentials*, *Phys. Lett.* **B795** (2019) 15 [1812.08235].

[4] H.T. Ding et al., *Chiral Phase Transition Temperature in (2+1)-Flavor QCD*, *Phys. Rev. Lett.* **123** (2019) 062002 [1903.04801].

[5] R.D. Pisarski and F. Wilczek, *Remarks on the Chiral Phase Transition in Chromodynamics*, *Phys.Rev.* **D29** (1984) 338.

[6] A. Butti, A. Pelissetto and E. Vicari, *On the nature of the finite temperature transition in QCD*, *JHEP* **08** (2003) 029 [hep-ph/0307036].

[7] M. Grahl, $U(2)_A U(2)_V$*-symmetric fixed point from the functional renormalization group*, *Phys. Rev.* **D90** (2014) 117904 [1410.0985].

[8] M.I. Buchoff, M. Cheng, N.H. Christ, H.T. Ding, C. Jung et al., *QCD chiral transition, U(1)A symmetry and the dirac spectrum using domain wall fermions*, *Phys.Rev.* **D89** (2014) 054514 [1309.4149].

[9] A. Bazavov et al., *Meson screening masses in (2+1)-flavor QCD*, *Phys. Rev. D* **100** (2019) 094510 [1908.09552].

[10] H. Ohno, U. Heller, F. Karsch and S. Mukherjee, $U_A(1)$ *breaking at finite temperature from the Dirac spectrum with the dynamical HISQ action*, *PoS* **LATTICE2012** (2012) 095 [1211.2591].

[11] V. Dick, F. Karsch, E. Laermann, S. Mukherjee and S. Sharma, *Microscopic origin of* $U_A(1)$ *symmetry violation in the high temperature phase of QCD*, *Phys. Rev.* **D91** (2015) 094504 [1502.06190].

[12] A. Tomiya, G. Cossu, S. Aoki, H. Fukaya, S. Hashimoto, T. Kaneko et al., *Evidence of effective axial U(1) symmetry restoration at high temperature QCD*, *Phys. Rev. D* **96** (2017) 034509 [1612.01908].

[13] JLQCD collaboration, *Study of the axial* $U(1)$ *anomaly at high temperature with lattice chiral fermions*, *Phys. Rev. D* **103** (2021) 074506 [2011.01499].

[14] S. Aoki, H. Fukaya and Y. Taniguchi, *Chiral symmetry restoration, eigenvalue density of Dirac operator and axial U(1) anomaly at finite temperature*, *Phys.Rev.* **D86** (2012) 114512 [1209.2061].

[15] G. 't Hooft, *Symmetry Breaking Through Bell-Jackiw Anomalies*, *Phys. Rev. Lett.* **37** (1976) 8.

PoS(LATTICE2021)619

[16] HotQCD collaboration, *The chiral transition and $U(1)_A$ symmetry restoration from lattice QCD using Domain Wall Fermions*, *Phys.Rev.* **D86** (2012) 094503 [1205.3535].

[17] D.J. Gross, R.D. Pisarski and L.G. Yaffe, *QCD and Instantons at Finite Temperature*, *Rev. Mod. Phys.* **53** (1981) 43.

[18] T. Kanazawa and N. Yamamoto, *Quasi-instantons in QCD with chiral symmetry restoration*, *Phys. Rev.* **D91** (2015) 105015 [1410.3614].

[19] G. Cossu, S. Aoki, H. Fukaya, S. Hashimoto, T. Kaneko et al., *Finite temperature study of the axial U(1) symmetry on the lattice with overlap fermion formulation*, *Phys.Rev.* **D87** (2013) 114514 [1304.6145].

[20] JLQCD collaboration, *Axial U(1) symmetry and mesonic correlators at high temperature in $N_f = 2$ lattice QCD*, in *37th International Symposium on Lattice Field Theory (Lattice 2019) Wuhan, Hubei, China, June 16-22, 2019*, 2020 [2001.07962].

[21] T. Kanazawa and N. Yamamoto, *U (1) axial symmetry and Dirac spectra in QCD at high temperature*, *JHEP* **01** (2016) 141 [1508.02416].

[22] H.T. Ding, S.T. Li, S. Mukherjee, A. Tomiya, X.D. Wang and Y. Zhang, *Correlated Dirac Eigenvalues and Axial Anomaly in Chiral Symmetric QCD*, *Phys. Rev. Lett.* **126** (2021) 082001 [2010.14836].

[23] H.-T. Ding, O. Kaczmarek, F. Karsch, S.-T. Li, S. Mukherjee, A. Tomiya et al., *Dirac Eigenvalue spectrum of N_f=2+1 QCD towards the chiral limit using HISQ fermions*, in *Proceedings, 37th International Symposium on Lattice Field Theory (Lattice 2019): Wuhan, China, June 16-22 2019*, 2019 [2001.05217].

[24] L. Giusti and M. Luscher, *Chiral symmetry breaking and the Banks-Casher relation in lattice QCD with Wilson quarks*, *JHEP* **03** (2009) 013 [0812.3638].

[25] G. Cossu, H. Fukaya, S. Hashimoto, T. Kaneko and J.-I. Noaki, *Stochastic calculation of the Dirac spectrum on the lattice and a determination of chiral condensate in 2+1-flavor QCD*, *PTEP* **2016** (2016) 093B06 [1607.01099].

[26] H.T. Ding, S.T. Li, A. Tomiya, X.D. Wang and Y. Zhang, *Chiral properties of (2+1)-flavor QCD in strong magnetic fields at zero temperature*, *Phys. Rev. D* **104** (2021) 014505 [2008.00493].

[27] C. Bernard, M. Golterman, Y. Shamir and S.R. Sharpe, *Comment on 'Chiral anomalies and rooted staggered fermions'*, *Phys. Lett. B* **649** (2007) 235 [hep-lat/0603027].

PoS(LATTICE2021)619